CHEMISTRY OF MATERIALS
Cite This: Chem. Mater. 2019, 31, 4325−4329
Communication
pubs.acs.org/cm

Generalized Synthesis of Uniform Metal Nanoparticles Assisted with Tungsten Hexacarbonyl

Xixia Zhao,[†,‡,#] Qian Di,[†,‡,#] Mingrui Li,[†] Qi Yang,[†] Ziyun Zhang,[†] Xinyang Guo,[†] Xiaokun Fan,[†] Kerong Deng,[†] Wen Chen,[†] Jun Zhang,[‡] Jiye Fang,[§] and Zewei Quan*[,†]

[†]Department of Chemistry, Southern University of Science and Technology (SUSTech), Shenzhen, Guangdong 518055, P. R. China
[‡]State Key Laboratory of Heavy Oil Processing, College of Chemical Engineering, China University of Petroleum, Qingdao, Shandong 266580, P. R. China
[§]Department of Chemistry, State University of New York at Binghamton, Binghamton, New York 13902, United States

Supporting Information

Metals represent more than two-thirds of the elements in the periodic table, and they have attracted extensive attention owing to their particular physical and chemical properties. Many metals at the nanoscale exhibit widespread applications, ranging from catalysis to electronics, photonics, energy conversion/storage, superconduction, and medicine.[1−8] For unambiguous identification of metal nanoparticle properties, the synthesis of uniform metal nanoparticles with well-defined size, shape, composition, and crystal structure is indispensable.[9−18] Up to now, a series of methods have been developed to prepare metal nanoparticles, among which colloidal synthesis has some advantages in the controlled synthesis of monodisperse metal nanoparticles.[19−28] In most cases, a metal salt precursor is controllably reduced in the presence of organic ligands, which prevent particle aggregation and improve the chemical stability of metal nanoparticles. However, the different reduction potentials of metal cations intrinsically limit the development of a versatile synthetic method for various metal nanoparticles. In addition, the need to regulate the nucleation and growth of metal nanoparticles often requires the use of some specific reducing agents or precursors, some of which are flammable and/or hazardous.[29] Therefore, developing a generalized approach for the synthesis of various uniform metal nanoparticles is highly desired for both fundamental research and practical applications.

Herein, we present a versatile strategy of uniform metal nanoparticles via the tungsten hexacarbonyl ($W(CO)_6$)-assisted reduction of different metal salts. The unique characteristics of $W(CO)_6$ make it possible to obtain 10 different kinds of uniform metal nanoparticles without size selection, ranging from transition metals to main group metals. Furthermore, the size of these metal nanoparticles can be readily tuned by adjusting reaction parameters. This method is further demonstrated to prepare uniform binary metal (e.g., Ag−Pd and Pd−Ni) nanoparticles.

The demonstration of this generalized synthetic strategy for various metal nanoparticles is shown in Figure 1. During the syntheses of these metal nanoparticles, the metal salt precursors are controllably reduced in the presence of $W(CO)_6$ and high boiling point solvents such as oleylamine (OAm) and/or oleic acid (OA), to produce corresponding metal nanoparticles. We start the discussion with the synthesis of Ag nanoparticles. In a typical synthesis, $W(CO)_6$, $AgNO_3$, OAm, tri-n-octylphosphine (TOP), and 1-octadecene (ODE) are mixed in a three-neck round-bottom flask at room temperature, and then the mixture is heated under an argon stream. These as-obtained Ag nanoparticles show the quasi-spherical shape with an average diameter of 16.9 ± 1.3 nm (Figure 1A). Furthermore, the size of Ag nanoparticles can be tuned to 10.8 ± 0.8 nm and 4.9 ± 0.9 nm with narrow size distributions by adjusting the capping ligands such as TOP and 1-dodecanethiol (DDT), respectively (Figures S1 and S2). Analogously, the $W(CO)_6$-assisted reaction method can also be extended to the synthesis of other noble metals with narrow size distributions such as Au (5.8 ± 0.6 nm, Figures 1B and S3) and Pd (12.7 ± 0.7 nm, 4.6 ± 0.4 nm, 2.6 ± 0.4 nm, Figures 1C, S4, and S5).

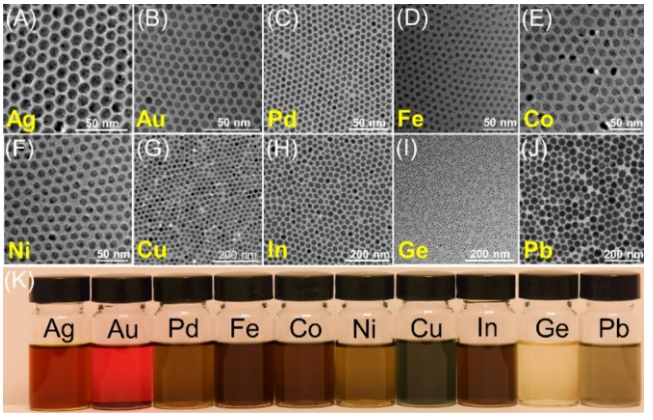

Figure 1. TEM images of as-obtained metal nanoparticles: (A) Ag; (B) Au; (C) Pd; (D) Fe; (E) Co; (F) Ni; (G) Cu; (H) In; (I) Ge; and (J) Pb. (K) Photos of 10 types of metal nanoparticles dispersed in hexane.

The syntheses of the first-row transition metal nanoparticles (e.g., Ni, Co, Fe, Cu) have been extensively studied, due to their catalysis, magnetic, and optics applications.[5,12] As for these relatively reactive metals, a strong reducing agent (e.g., superhydride) is usually necessary at elevated temperature to reduce metal precursors. In this work, this $W(CO)_6$-assisted

Received: January 17, 2019
Revised: March 21, 2019
Published: March 26, 2019

DOI: 10.1021/acs.chemmater.9b00219
Chem. Mater. 2019, 31, 4325−4329

method is successfully developed to prepare several monodisperse first-row transition metal nanoparticles including Fe (6.9 ± 0.8 nm), Co (13.4 ± 1.4 nm, 8.5 ± 0.9 nm), Ni (13.0 ± 1.2 nm, 7.9 ± 0.8 nm), and Cu (19.5 ± 2.3 nm) (Figures 1D−G and S6−S11), under reaction conditions similar to those for noble metal nanoparticles. Furthermore, instead of using toxic, expensive organometallic compounds (e.g., $Fe[N(SiMe_3)_2]_2$) as metal precursors, we chose inexpensive and environmentally friendly compounds, namely, metal chlorides (or metal acetates) in our experiments (refer to Experimental Section for details).

Compared to transition metal nanoparticles as described above, the syntheses of group III and IV metal nanoparticles are relatively less explored.[30] First, strong reducing agents are necessary for the formation of such metal nanoparticles, due to their negative redox potentials. Second, the uniformity of these metal nanoparticles is difficult to control because of their low affinity with most commonly used organic ligands in nanoparticle syntheses such as amines and phosphines. In addition, thiols or long-chain carboxylic acids can react with those elements at high temperature. Third, some bulk main group metals (e.g., In and Pb) have low melting points, preventing the controlled formation of those metal nanoparticles at high temperature. Our results indicate that this $W(CO)_6$-assisted procedure is applicable to the syntheses of main group metal nanoparticles with narrow size distributions such as In (22.5 ± 3.1 nm), Ge (6.0 nm ±1.1 nm), and Pb (34.4 ± 4.7 nm, 16.6 ± 3.4 nm) (Figures 1H−J and S12−16), greatly simplifying the selection of reducing agents and capping ligands. As shown in Figure 1K, all these as-prepared metal nanoparticles can be well dispersed in hexane, forming stable colloidal solutions.

In addition to single metal nanoparticles, this $W(CO)_6$-assisted synthetic method can also be extended to the synthesis of binary metal nanoparticles. In a typical synthesis, high-quality monodisperse Ag−Pd and Pd−Ni nanoparticles can be obtained by directly heating the mixture of $W(CO)_6$, $Pd(acac)_2$, $AgNO_3$ (or $Ni(CH_3COO)_2$), and OAm under argon flow. TEM images of $Ag_{87}Pd_{13}$ (Figure 2A) and $Pd_{85}Ni_{15}$ (Figure 2D) nanoparticles show near-spherical particles with narrow size distributions. The corresponding HRTEM images (insets) and XRD patterns (Figures 2C,F) suggest the good

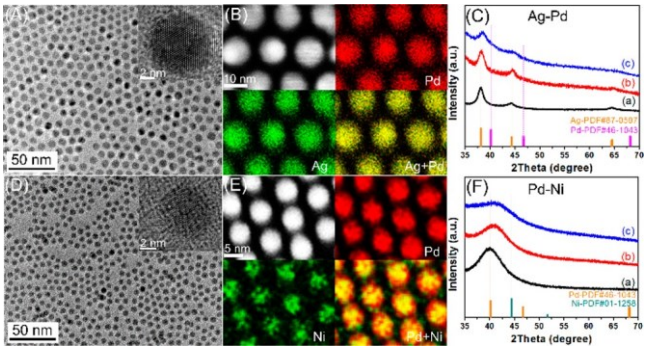

Figure 2. TEM images of (A) $Ag_{87}Pd_{13}$ and (D) $Pd_{85}Ni_{15}$ nanoparticles with insets showing their HRTEM images. Elemental mapping images of (B) $Ag_{87}Pd_{13}$ and (E) $Pd_{85}Ni_{15}$ nanoparticles. (C) XRD patterns of Ag−Pd nanoparticles with different ratios: (a) Ag; (b) $Ag_{87}Pd_{13}$; and (c) $Ag_{78}Pd_{22}$. (F) XRD patterns of Pd−Ni nanoparticles with different ratios: (a) Pd; (b) $Pd_{85}Ni_{15}$; and (c) $Pd_{53}Ni_{47}$.

crystallinity of these binary metal nanoparticles. Elemental mapping images in Figure 2B clearly confirm that Ag and Pd are evenly distributed in the $Ag_{87}Pd_{13}$ nanoparticles, and their atomic mole percentages are determined by the inductively coupled plasma mass spectrometry (ICP-MS). However, surface segregation of Pd on $Pd_{85}Ni_{15}$ nanoparticles can be observed in Figure 2E, which is a common phenomenon in Pd-based binary alloys. It has been revealed that many factors such as mixing enthalpy, temperature, crystal orientation on the surface, and elastic strain energy, could have an influence on the surface segregation behavior of Pd-based binary alloys.[31−33] The components of Ag−Pd and Pd−Ni nanoparticles can be conveniently tuned by the precursor concentration, and thus monodisperse $Ag_{78}Pd_{22}$ and $Pd_{53}Ni_{47}$ nanoparticles can also be obtained. With the variations of atomic percentages, diffraction peaks of these binary metal nanoparticles are shifted correspondingly (Figure 2C,F). These results indicate that the $W(CO)_6$-assisted reduction process is a versatile synthetic method for both monodisperse single metal and binary metal nanoparticles (Table S1).

To intrinsically understand the functions of $W(CO)_6$ in these syntheses, we have rationally designed a series of control experiments, as shown in Table 1. First of all, $W(CO)_6$ is

Table 1. Comparison of Experimental Results under Different Reaction Conditions

metal	$W(CO)_6$	without $W(CO)_6$	CO
Ag	4.9 nm	1.5−7.0 nm	1.5−6.5 nm
Au	5.8 nm	4.6−15.0 nm	4.0−12.7 nm
Pd	12.7 nm	8 nm	2−5 nm
Fe	6.9 nm	200−300 nm	84−426 nm
Co	8.5 nm	20−70 nm	Co and CoO
Ni	7.9 nm	2−17 nm	no product
Cu	19.5 nm	18−80 nm	10−20 nm
In	22.5 nm	In and In_2O_3	no product
Ge	6.0 nm	no product	∼9 nm
Pb	16.6 nm	no product	no product

removed while keeping all other conditions unchanged, and in this case OAm becomes the only reducing agent in the reactions. In the absence of $W(CO)_6$, OAm itself is strong enough to reduce some metal cations into zerovalent metals except for Ge and Pb. For example, OAm can reduce Au^{3+} to Au^0 at elevated temperature, which has also been reported.[34,35] However, Au nanoparticles with broad size distribution ($\sigma \approx 21\%$) are produced in the absence of $W(CO)_6$ in our system (Figure S17D). In contrast, the reaction proceeds faster in the presence of $W(CO)_6$, and the size distribution is greatly narrowed ($\sigma \approx 10\%$) (Figure S17E). Such results indicate that the addition of $W(CO)_6$ may promote the faster nucleation of Au nanoparticles, which is essential to produce uniform Au nanoparticles. Similar results also can be found in the cases of other metal nanoparticles including Ag, Pd, Fe, Co, Ni, Cu, and In (Figures S17 and S18). Notably, the formations of Fe, Co, and Cu nanoparticles become very difficult to control without $W(CO)_6$, because of their slow nucleation kinetics (Figures S17J and S18A,G). It is reasonable to conclude that $W(CO)_6$ plays an essential role in the nucleation and growth of those metal nanoparticles, leading to the formation of monodisperse metal nanoparticles.

The significant effects of $W(CO)_6$ on the syntheses of uniform metal nanoparticles should originate from CO gas

DOI: 10.1021/acs.chemmater.9b00219
Chem. Mater. 2019, 31, 4325−4329

and/or W^0 species that are in situ generated in solution at elevated temperature. To explicitly understand the individual roles of CO gas and W^0 species, we have also carried out another set of control experiments, in which CO gas is continuously introduced into the solution as the reducing agent to replace $W(CO)_6$. Compared with the cases in the absence of $W(CO)_6$, similar experiment results (irregular shape and/or broad size distribution) are obtained for Ag, Au, Fe, Cu, Pd, and Co nanoparticle systems (Table 1 and Figure S19). It should be noted that the mixture of smaller Co (<5 nm) and CoO nanoparticles (Figures S19K,L) is produced in this situation, and the formation of CoO nanoparticles is probably due to the severe oxidation of tiny Co nanoparticles in the air.[36] Instead of no Ge nanoparticles produced without $W(CO)_6$, the introduction of CO gas results in the formation of Ge nanoparticles, indicating CO is a stronger reducing agent than OAm to reduce Ge^{2+} to Ge atom (Figure S20). However, CO gas is still not strong enough to reduce Pb^{2+} cations, and therefore no Pb nanoparticles are produced in this case, as shown in Table 1. As discussed above, OAm itself is strong enough to produce Ni and In nanoparticles although with poor morphology uniformity. However, no nanoparticles are obtained in the control experiments of Ni and In metals when introducing CO gas into the reactions. It is hypothesized that there would be some metal carbonyls (e.g., $Ni(CO)_4$) produced during the reactions, which can be obtained via the reaction of metal clusters and CO under the synthesis condition.[37,38] As a strong coordination ligand, CO can form coordination complexes with some metals through the strong coordinate covalent bond, especially in the cases of In and Ni.[39−42] Hence, indium carbonyl and nickel carbonyl with high bond stability are very stable and not easily decomposed compared to other metal carbonyls in our system. As a result, the nucleation and growth of In and Ni nanoparticles are seriously inhibited when using CO gas as a reducing agent. However, uniform Ni and In nanoparticles are still obtained in this $W(CO)_6$-assisted method. Thus, the presence of W^0 species from the decomposition of $W(CO)_6$ is probably essential in the formation of these metal nanoparticles, especially for In and Ni ones.

We speculate that the W^0 may act as a sacrificial reducing agent to facilitate the rapid reduction of metal ions to metal atoms in the nucleation stage. By comparing redox potentials (vs SHE) of different metal ion/metal pairs (Table S2), the W^{6+}/W pair has a more negative reduction potential than those of Au^{3+}/Au, Pd^{2+}/Pd, Ag^{+}/Ag, Cu^{2+}/Cu, and Ge^{2+}/Ge pairs. So, it is reasonable that W^0 can reduce Au^{3+}, Pd^{2+}, Ag^{+}, Cu^{2+}, and Ge^{2+} to zero-valence metals in this system. In contrast, it seems impossible for the reduction of Pb^{2+}, Ni^{2+}, Co^{2+}, In^{3+}, and Fe^{2+} by W^0 according to their redox potentials.

However, the UV−vis absorption (Figure S21) results of $W(CO)_6$ decomposition and the nucleation stage of Ni nanoparticles in the presence of $W(CO)_6$ indicate that the redox reactions between W^0 and these metal cations may also occur. As shown in Figure S21A (red line), two absorption peaks at 352 and 380 nm appear after $W(CO)_6$ decomposes. We think that these peaks originate from the WO_x clusters because of the rapid oxidation of W^0 species decomposed from $W(CO)_6$, which can be further supported by its photoluminescence spectrum excited at 380 nm in Figure S21B, which is similar to WO_x ultrathin nanowires.[43] When Ni^{2+} precursor is introduced into the system, the spectrum is different compared to that of $W(CO)_6$ decomposition. As the temperature increases to 220 °C, the peaks of WO_x clusters disappear unexpectedly (Figure S21a, blue line), indicating the complete consumption of W^0 species during the nucleation stage of Ni nanoparticles. This result provides strong evidence for our speculation that W^0 could act as a sacrificial reducing agent in the nucleation stage of metal nanoparticles, even for those more reactive metals.

This phenomenon should be ascribed to the enhanced reduction ability of W^0 due to its ultrasmall characteristic. It has been reported that the oxidation potential of metal nanoparticles would dramatically decrease due to the confinement effect.[44,45] For example, when particle size decreases to less than 3 nm, Ag and Au can react with more reactive metal ions, such as Cu^{2+} and Ag^{+}, known as "antigalvanic reaction".[46] Therefore, it is reasonable to speculate that tiny W^0 species can act as an effective sacrificial reducing agent during the syntheses of these metals. In addition, according to the X-ray photoelectron spectroscopy (XPS) results (Figure S22), the W species on all these representatives metal nanoparticles (Pd, Ni, In, Pb) have a positive valence (+6), confirming that W^0 species can be oxidized by all these metal cations. Notably, through ligand exchange processes (refer to the Experimental Section in Supporting Information for details), the content of W element in the final products can be reduced to as low as 0.13 atom % (Table S3, Figure S23). The positive valence and efficient removal of W element both indicate that the residual W species are absorbed on metal particle surface as ligands rather than alloying with them.

Based on these experiments, the intriguing roles of $W(CO)_6$ in the syntheses of uniform metal nanoparticles are clearly revealed. The $W(CO)_6$-assisted reaction process should proceed in the following steps (Figure 3). (i) Decomposition of $W(CO)_6$: CO and W^0 species are generated through the rapid decomposition of $W(CO)_6$ at elevated temperature (>140 °C) before the reduction of metal salts. (ii) Reduction of metal salts: with the assistance of CO, W^0 species, and OAm, metal salts with positive valence (M^{n+}, $n = 1-3$) are reduced to zerovalent metals (M^0). (iii) Formation and decomposition of metal carbonyls ($M_x(CO)_y$): metal carbonyls are formed by CO binding to metals with dative bond and along with the tendency of decomposition at appropriate temperature. (iv) Formation of uniform metal nanoparticles: the growth of metal nanoparticles continues in the presence of CO and other ligands to regulate their morphology and size.

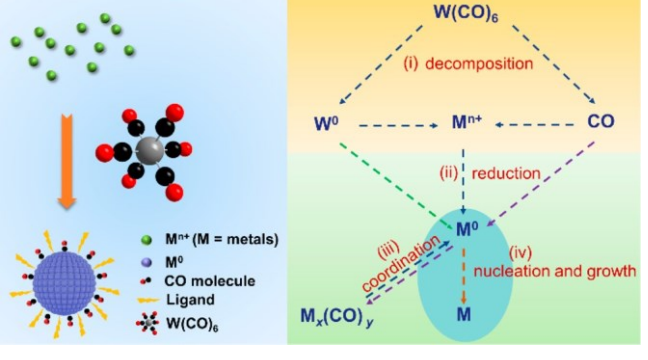

Figure 3. Schematic diagrams illustrating the mechanism of the $W(CO)_6$-assisted reaction process for the formation of different metal nanoparticles.

DOI: 10.1021/acs.chemmater.9b00219
Chem. Mater. 2019, 31, 4325−4329

In summary, we have developed a generalized strategy for the controlled syntheses of the 10 monodisperse metals through the $W(CO)_6$-assisted reduction of various metal salts in organic phase solution. By adjusting reaction parameters, the size of these metal nanoparticles can be readily controlled without size selection. Based on a series of control experiments, $W(CO)_6$ is revealed to play a crucial role in the syntheses of uniform metal nanoparticles, greatly simplifying the selection of reducing agents and capping ligands. The strategy not only is applicable to single transition metals and main group metals but also can be extended to binary metals as well. It represents a novel versatile approach to synthesize different kinds of metal nanoparticles, promoting the investigations of their various applications.

ASSOCIATED CONTENT

Supporting Information

The Supporting Information is available free of charge on the ACS Publications website at DOI: 10.1021/acs.chemmater.9b00219.

Additional data from XRD, TEM, EDS, ICP-MS, and XPS and experimental details for the controlled synthesis of uniform metal nanoparticles (PDF)

AUTHOR INFORMATION

Corresponding Author

*(Z.Q.) E-mail: quanzw@sustech.edu.cn.

ORCID

Zewei Quan: 0000-0003-1998-5527

Author Contributions

Z.Q., J.Z., and J.F. proposed the research direction and guided the project. X.Z. and Q.D. designed the experiments, collected all electron microscopy data, performed the analysis, and wrote the paper. X.Z., Q.D., Q.Y., Z.Z., and X.G. performed the material synthesis and characterization. M.L., X.F., K.D., and W.C. performed the component characterization. All authors discussed the results and commented on the manuscript.

Author Contributions

#(X.Z. and Q.D.) These authors contributed equally to this work.

Notes

The authors declare no competing financial interest.

ACKNOWLEDGMENTS

This work was supported by the National Natural Science Foundation of China (NSFC) (No. 51772142), Development and Reform Commission of Shenzhen Municipality (Novel Nanomaterial Discipline Construction Plan), and Shenzhen Science and Technology Innovation Committee (Nos. JCYJ20170412152528921, KQJSCX20170328155428476). J.F. acknowledges the financial support from NSF (DMR-1808383).

REFERENCES

(1) Zhang, H.; Jin, M.; Xia, Y. Noble-Metal Nanocrystals with Concave Surfaces: Synthesis and Applications. Angew. Chem., Int. Ed. 2012, 51, 7656−7673.

(2) Chen, Y.; Fan, Z.; Zhang, Z.; Niu, W.; Li, C.; Yang, N.; Chen, B.; Zhang, H. Two Dimensional Metal Nanomaterials: Synthesis, Properties, and Applications. Chem. Rev. 2018, 118, 6409−6455.

(3) Guo, S.; Wang, E. Noble Metal Nanomaterials: Controllable Synthesis and Application in Fuel Cells and Aanalytical Sensors. Nano Today 2011, 6, 240−264.

(4) Wang, D.; Li, Y. Bimetallic Nanocrystals: Liquid-Phase Synthesis and Catalytic Applications. Adv. Mater. 2011, 23, 1044−1060.

(5) Wu, L.; Mendoza-Garcia, A.; Li, Q.; Sun, S. Organic Phase Syntheses of Magnetic Nanoparticles and Their Applications. Chem. Rev. 2016, 116, 10473−10512.

(6) Fan, Z.; Zhang, H. Template Synthesis of Noble Metal Nanocrystals with Unusual Crystal Structures and Their Catalytic Applications. Acc. Chem. Res. 2016, 49, 2841−2850.

(7) Stowell, C. A.; Korgel, B. A. Iridium Nanocrystal Synthesis and Surface Coating-Dependent Catalytic Activity. Nano Lett. 2005, 5, 1203−1207.

(8) Huang, X.; Tang, S.; Mu, X.; Dai, Y.; Chen, G.; Zhou, Z.; Ruan, F.; Yang, Z.; Zheng, N. Freestanding Palladium Nanosheets with Plasmonic and Catalytic Properties. Nat. Nanotechnol. 2011, 6, 28.

(9) Quan, Z.; Wang, Y.; Fang, J. High-Index Faceted Noble Metal Nanocrystals. Acc. Chem. Res. 2013, 46, 191−202.

(10) Zhang, J.; Fang, J. A General Strategy for Preparation of Pt 3d-Transition Metal (Co, Fe, Ni) Nanocubes. J. Am. Chem. Soc. 2009, 131, 18543−18547.

(11) Pang, X.; He, Y.; Jung, J.; Lin, Z. 1D Nanocrystals with Precisely Controlled Dimensions, Compositions, and Architectures. Science 2016, 353, 1268−1272.

(12) Murray, C. B.; Sun, S.; Doyle, H.; Betley, T. Monodisperse 3d Transition-Metal (Co,Ni,Fe) Nanoparticles and Their Assembly into Nanoparticle Superlattices. MRS Bull. 2001, 26, 985−991.

(13) Zhao, X.; Di, Q.; Wu, X.; Liu, Y.; Yu, Y.; Wei, G.; Zhang, J.; Quan, Z. Mild Synthesis of Monodisperse Tin Nanocrystals and Tin Chalcogenide Hollow Nanostructures. Chem. Commun. 2017, 53, 11001−11004.

(14) Sun, Y.; Xia, Y. Shape-Controlled Synthesis of Gold and Silver Nanoparticles. Science 2002, 298, 2176−2179.

(15) Wu, J.; Gross, A.; Yang, H. Shape and Composition-Controlled Platinum Alloy Nanocrystals Using Carbon Monoxide as Reducing Agent. Nano Lett. 2011, 11, 798−802.

(16) Langille, M. R.; Personick, M. L.; Zhang, J.; Mirkin, C. A. Defining Rules for the Shape Evolution of Gold Nanoparticles. J. Am. Chem. Soc. 2012, 134, 14542−14554.

(17) Wu, Z.; Jin, R. On the Ligand's Role in the Fluorescence of Gold Nanoclusters. Nano Lett. 2010, 10, 2568−2573.

(18) Nolan, B. M.; Chan, E. K.; Zhang, X.; Muthuswamy, E.; van Benthem, K.; Kauzlarich, S. M. Sacrificial Silver Nanoparticles: Reducing GeI_2 To Form Hollow Germanium Nanoparticles by Electroless Deposition. ACS Nano 2016, 10, 5391−5397.

(19) He, M.; Protesescu, L.; Caputo, R.; Krumeich, F.; Kovalenko, M. V. A General Synthesis Strategy for Monodisperse Metallic and Metalloid Nanoparticles (In, Ga, Bi, Sb, Zn, Cu, Sn, and Their Alloys) via in Situ Formed Metal Long-Chain Amides. Chem. Mater. 2015, 27, 635−647.

(20) Wang, X.; Zhuang, J.; Peng, Q.; Li, Y. A General Strategy for Nanocrystal Synthesis. Nature 2005, 437, 121.

(21) Xia, Y.; Gilroy, K. D.; Peng, H.-C.; Xia, X. Seed-Mediated Growth of Colloidal Metal Nanocrystals. Angew. Chem., Int. Ed. 2017, 56, 60−95.

(22) Zhang, Q.; Li, N.; Goebl, J.; Lu, Z.; Yin, Y. A Systematic Study of the Synthesis of Silver Nanoplates: Is Citrate a "Magic" Reagent? J. Am. Chem. Soc. 2011, 133, 18931−18939.

(23) Pang, X.; Zhao, L.; Han, W.; Xin, X.; Lin, Z. A General and Robust Strategy for the Synthesis of Nearly Monodisperse Colloidal Nanocrystals. Nat. Nanotechnol. 2013, 8, 426.

(24) Chockla, A. M.; Harris, J. T.; Korgel, B. A. Colloidal Synthesis of Germanium Nanorods. Chem. Mater. 2011, 23, 1964−1970.

(25) Tao, A. R.; Habas, S.; Yang, P. Shape Control of Colloidal Metal Nanocrystals. Small 2008, 4, 310−325.

(26) Grzelczak, M.; Perez-Juste, J.; Mulvaney, P.; Liz-Marzan, L. M. Shape Control in Gold Nanoparticle Synthesis. Chem. Soc. Rev. 2008, 37, 1783−1791.

DOI: 10.1021/acs.chemmater.9b00219
Chem. Mater. 2019, 31, 4325−4329

(27) Sau, T. K.; Rogach, A. L. Nonspherical Noble Metal Nanoparticles: Colloid-Chemical Synthesis and Morphology Control. Adv. Mater. 2010, 22, 1781−1804.
(28) Gu, J.; Zhang, Y.-W.; Tao, F. Shape Control of Bimetallic Nanocatalysts through Well-Designed Colloidal Chemistry Approaches. Chem. Soc. Rev. 2012, 41, 8050−8065.
(29) Dumestre, F.; Chaudret, B.; Amiens, C.; Renaud, P.; Fejes, P. Superlattices of Iron Nanocubes Synthesized from $Fe[N(SiMe_3)_2]_2$. Science 2004, 303, 821−823.
(30) Zolotavin, P.; Guyot-Sionnest, P. Meissner Effect in Colloidal Pb Nanoparticles. ACS Nano 2010, 4, 5599−5608.
(31) Zhao, M.; Sloof, W. G.; Böttger, A. J. Modelling of Surface Segregation for Palladium Alloys in Vacuum and Gas Environments. Int. J. Hydrogen Energy 2018, 43, 2212−2223.
(32) Batirev, I. G.; Leiro, J. A. Surface Segregation of PdRh, PdNi and PdCo Alloys. J. Electron Spectrosc. Relat. Phenom. 1995, 71, 79−86.
(33) Løvvik, O. Surface Segregation in Palladium Based Alloys from Density-Functional Calculations. Surf. Sci. 2005, 583, 100−106.
(34) Hiramatsu, H.; Osterloh, F. E. A Simple Large-Scale Synthesis of Nearly Monodisperse Gold and Silver Nanoparticles with Adjustable Sizes and with Exchangeable Surfactants. Chem. Mater. 2004, 16, 2509−2511.
(35) Peng, S.; McMahon, J. M.; Schatz, G. C.; Gray, S. K.; Sun, Y. Reversing the Size-Dependence of Surface Plasmon Resonances. Proc. Natl. Acad. Sci. U. S. A. 2010, 107, 14530.
(36) Sun, S.; Murray, C. B. Synthesis of Monodisperse Cobalt Nanocrystals and Their Assembly into Magnetic Superlattices. J. Appl. Phys. 1999, 85, 4325−4330.
(37) Wei, G.; Zhao, X.; An, C.; Liu, J.; Wang, Z.; Du, K.; Zhang, J. In Situ Thermolysis of Pt-Carbonyl Complex to Form Supported Clean Pt Nanoclusters with Enhanced Catalytic Performance. Sci. China Mater. 2017, 60, 131−140.
(38) Spessard, G. O.; Miessler, G. L. In Organometallic Chemistry; Oxford University Press: Oxford, 2010; p 84.
(39) Jiang, Y.; Lee, T.; Rose-Petruck, C. G. Structure of Solvated $Fe(CO)_5$: FTIR Measurements and Density Functional Theory Calculations. J. Phys. Chem. A 2003, 107, 7524−7538.
(40) Gajdoš, M.; Eichler, A.; Hafner, J. CO Adsorption on Close-Packed Transition and Noble Metal Surfaces: Trends from ab Initio Calculations. J. Phys.: Condens. Matter 2004, 16, 1141.
(41) Himmel, H. J.; Downs, A. J.; Green, J. C.; Greene, T. M. Thermal and Photolytic Reactions of Gallium and Indium Atoms (M) and Their Dimers M_2 with Carbon Monoxide in Low-Temperature Matrices: Formation of Terminal, Bridged, and Ionic Carbonyl Derivatives. J. Phys. Chem. A 2000, 104, 3642−3654.
(42) Jiang, L.; Xu, Q. Observation of the Lead Carbonyls, Pb_nCO (n = 1−4):Pb_nCO (n = 1−4): Reactions of Lead Atoms and Small Clusters with Carbon Monoxide in Solid Argon. J. Chem. Phys. 2005, 122, 034505.
(43) Moshofsky, B.; Mokari, T. Length and Diameter Control of Ultrathin Nanowires of Substoichiometric Tungsten Oxide with Insights into the Growth Mechanism. Chem. Mater. 2013, 25, 1384−1391.
(44) Gan, Z.; Xia, N.; Wu, Z. Discovery, Mechanism, and Application of Antigalvanic Reaction. Acc. Chem. Res. 2018, 51, 2774−2783.
(45) Wang, M.; Wu, Z.; Chu, Z.; Yang, J.; Yao, C. Chemico-Physical Synthesis of Surfactant- and Ligand-Free Gold Nanoparticles and Their Anti-Galvanic Reduction Property. Chem. - Asian J. 2014, 9, 1006−1010.
(46) Wu, Z. Anti-Galvanic Reduction of Thiolate-Protected Gold and Silver Nanoparticles. Angew. Chem. 2012, 124, 2988−2992.

DOI: 10.1021/acs.chemmater.9b00219
Chem. Mater. 2019, 31, 4325−4329